Bahar Davoudi*, Kostadinka Bizheva, Alexander Wong, Robert Dinniwell, Wilfred Levin and Alex Vitkin

Correlating optical coherence tomography images with dose distribution in late oral radiation toxicity patients

Optische Kohärenztomographie in Korrelation mit der Dosisverteilung bei Patienten mit später oraler Radiotoxizität

Abstract

Background and objective: Late oral radiation toxicity occurs in about half of the patients who undergo head-and-neck radiotherapy, reducing the quality of life drastically. The total delivered radiation dose has been shown to be one of the predictors of these late complications. To demonstrate this, the studies carried out so far have used either visual observation together with symptom-based scoring systems or histology to evaluate the tissue response. However, the former lacks imaging information on tissue subsurface and the latter is invasive and exposes the patients to additional risks. Therefore, there is a need for a non-hazardous, non-invasive subsurface monitoring tool that can provide more objective information on dose-dependent response of normal oral tissue to radiation.

Materials and methods: To address this unmet clinical need, optical coherence tomography (OCT) was used. A clinical study was conducted on 14 late oral radiation toxicity patients and 5 age-matched healthy volunteers. OCT structural images were acquired from different oral regions in both cohorts and were then de-speckled in order to provide a better visualization of the subsurface layers and features. The alterations in patients' de-speckled OCT images compared to the healthy cohort are reviewed, and potential correlations between the total dose to specific regions and the abnormal features observed in the OCT images of the same sites are discussed.

Results: OCT images were acquired from 32 sites in 14 patients, 15 of these sites belonged to the regions which received >50 Gy radiation dose and the rest to the region which was irradiated to <50 Gy. The de-speckled OCT images from the former group showed major differences, such as total layer disruption, compared to the images of healthy oral tissue. The de-speckled OCT images from all but one of the regions which received <50 Gy showed normal features and layer definition compared to healthy oral OCT images. Same results were observed in an intra-patient comparison of the ipsilateral (dose >70 Gy) and contralateral (dose <25 Gy) soft palate of one of the patients, suggesting the results are independent of anatomical differences between individuals.

Conclusion: This preliminary clinical study showed the ability of OCT to differentiate subsurface features in the oral regions that received high radiation dose (>50 Gy) compared to healthy oral tissue. These results can be used to design a prospective study to monitor oral subsurface changes periodically (e.g., every 6 months) following radiotherapy, to further understand the mechanism of late radiation toxicity and its relation to dose.

Keywords: optical coherence tomography; late oral radiation toxicity; radiation late effects; fibrosis.

***Corresponding author: Bahar Davoudi,** Medical Biophysics Department, University of Toronto, MaRS/TMDT building, 101 College Street, 15th floor, Toronto, ON M5G 1L7, Canada, e-mail: bahar.davoudi@utoronto.ca

Kostadinka Bizheva: Department of Physics and Astronomy, University of Waterloo, 200 University Avenue West, Waterloo, ON N2L 3G1, Canada

Alexander Wong: Department of Systems Design Engineering, University of Waterloo, 200 University Avenue West, Waterloo, ON N2L 3G1, Canada

Robert Dinniwell and Wilfred Levin: Princess Margaret Cancer Center, 610 University Avenue, Toronto, ON M5G 2M9, Canada

Alex Vitkin: Medical Biophysics Department, University of Toronto, MaRS/TMDT building, 101 College Street, 15th floor, Toronto, ON M5G 1L7, Canada

Zusammenfassung

Hintergrund und Ziel: Späte orale Radiotoxizität tritt bei etwa der Hälfte der Patienten auf, die sich einer Strahlentherapie im Hals-Kopf-Bereich unterziehen müssen, und

führt zu einer drastischen Verschlechterung der Lebensqualität. Es hat sich gezeigt, dass die verabreichte Gesamtstrahlendosis einer der entscheidenden Prädiktoren für Spätfolgen ist. Um dies zu evaluieren, nutzten bisherige Untersuchungen entweder visuelle Beobachtungen in Kombination mit einem Symptom-basierten Scoring-System oder Histologien zur Beurteilung der Gewebereaktion. Beide Methoden sind limitiert; der ersteren fehlen Bildinformationen des Gewebeuntergrunds (SubSurface) und letztere ist invasiv und für die Patienten mit zusätzlichen Risiken verbunden. Daraus ergibt sich die Notwendigkeit für ein sicheres, nicht-invasives SubSurface-Monitoringverfahren, das mehr objektive Informationen über die dosisabhängige Reaktion des normalen oralen Gewebes auf Bestrahlung liefern kann.

Materialien und Methoden: Um den beschriebenen klinischen Bedarf aufzugreifen, wurde die optische Kohärenztomographie (optical coherence tomography, OCT) eingesetzt und eine klinische Studie an 14 an später oraler Radiotoxizität leidenden Patienten sowie 5 altersgleichen gesunden Probanden durchgeführt. Es wurden OCT-Bilder von verschiedenen Mundregionen in beiden Kohorten aufgenommen und entstört (de-speckled), um die unteren Gewebeschichten und Merkmale besser darzustellen. Anschließend wurden die entstörten OCT-Bilder der Patienten mit denen der gesunden Kohorte verglichen und mögliche Zusammenhänge zwischen der Gesamtstrahlendosis und den in den OCT-Bildern beobachteten abnormen Funktionen diskutiert.

Ergebnisse: Insgesamt wurden OCT-Bilder von 32 Lokalisationen in 14 Patienten akquiriert; 15 dieser Lokalisationen waren Geweberegionen zuzuordnen, die einer Strahlendosis von mehr als 50 Gy ausgesetzt waren. Die restlichen untersuchten Regionen wurden mit bis zu 50 Gy bestrahlt. Die entstörten OCT-Bilder der ersten Gruppe zeigten große Unterschiede, wie beispielsweise die totale Zerstörung der Gewebe-Schichtstruktur im Vergleich mit Bildern von gesundem oralem Gewebe. Hingegen zeigten die entstörten OCT-Bilder von den Regionen, die mit <50 Gy bestrahlt wurden, im Vergleich zur gesunden Mundschleimhaut eine normale Funktion und Schichtdefinition. Gleiche Ergebnisse wurden bei einem Intra-Patienten-Vergleich am weichen Gaumen eines Patienten – sowohl ipsilateral (Dosis >70 Gy) als auch kontralateral (Dosis <25 Gy) – beobachtet, was die Annahme unterstützt, dass die Ergebnisse unabhängig von inter-individuellen anatomischen Unterschieden sind.

Fazit: Die präsentierte klinische Studie belegt die Anwendbarkeit der OCT zur Differenzierung von unterhalb der Gewebeoberfläche liegenden Gewebemerkmalen im Mundbereich nach Exposition mit einer hohen Strahlendosis (>50 Gy) im Vergleich zu gesundem Gewebe. Diese Ergebnisse können verwendet werden, um eine prospektive Studie zur periodischen Überwachung oraler SubSurface-Gewebeveränderungen (z.B. alle sechs Monate) nach Strahlentherapie zu entwerfen, um den Mechanismus der späten Radiotoxizität in Korrelation mit der Strahlenddosis noch besser zu verstehen.

Schlüsselwörter: optische Kohärenztomographie; späte orale Radiotoxizität; Bestrahlungsspätfolgen; Fibrose.

DOI 10.1515/plm-2014-0022
Received June 12, 2014; revised July 21, 2014; accepted July 30, 2014; previously published online August 23, 2014

1 Introduction

Radiotherapy of head-and-neck cancer patients is associated with side effects to the normal oropharyngeal tissue that lies close to the tumor and adjacent lymphatics. This occurs because generally, accurate tumor margin delineation is impossible. Therefore, even though techniques such as intensity modulated radiotherapy (IMRT) [1] have improved beam delivery to the tumor, still the surrounding normal tissue receives relatively high radiation doses leading to normal tissue damage. Such damage to normal tissue either manifests during the course of treatment and within a few months following the treatment, or months and years after therapy is over. The former is called early toxicity and is prevalent in almost all patients receiving radiotherapy [2]. It resolves within several weeks to a few months [3, 4]. The latter, which is called late toxicity, occurs in about half of the patients [5] and can take up to years to heal [4]. The total delivered radiation dose has been shown to be one of the predictors of these late complications [6]. Therefore, late toxicities are important in determining the quality of life of head-and-neck cancer patients after radiotherapy [2].

The most common technique for either clinical diagnosis or performing research on the mechanism of radiation effects is through superficial oral tissue examination, interpreted using common scoring systems, such as Radiation Therapy Oncology Group (RTOG)/European Organization for Research and Treatment of Cancer (EORTC) [5]. Taking biopsies to better examine the subsurface alterations, is another technique that is mostly used for research purposes and seldom for clinical diagnosis due to augmented risk of infection, fistula formation, and tissue break down. Therefore, since the former technique cannot

reveal extensive subsurface information and the latter is invasive, there is a clinical and research need for a non-invasive non-hazardous subsurface imaging tool for monitoring late oral radiation toxicity. One can then monitor the response of subsurface oral tissue to various radiation doses to help establishing the onset of radiation effects as a function of dose, and to "shed light" on the mechanism of radiation-induced complications.

To address this clinical and research need, optical coherence tomography (OCT) has been used by a few research groups. OCT provides micron-scale resolution images to a depth of ~1–2 mm in most biological tissues [7]. Its volumetric grayscale images provide details on tissue microstructure, while its functional imaging modalities (such as Doppler [8] and speckle variance [9]) can help monitoring blood flow and mapping blood vasculature. Owing to these features and the possibility of integrating an OCT system into a fiber-optic probe, OCT has gained attention in monitoring a number of oral malignancies [10, 11] as well as radio/chemotherapy-induced mucositis (inflammation of oral mucosa, an early radiation/chemotherapy side effect) [12–15]. OCT has also been used to monitor early radiation side effects as a function of total delivered dose [12, 14]. In the current study, the correlation between the abnormalities in de-speckled OCT structural images of specific oral regions and the total dose delivered to the same region are discussed.

2 Materials and methods

2.1 Clinical study

The clinical study "Optical coherence tomography for monitoring late oral radiation toxicity after radiotherapy of head-and-neck cancer patients" (ClinicalTrials.gov identifier: NCT01692600 [16]) was approved by the Research Ethics Board of the Princess Margaret Cancer Center, Toronto, Canada. It has been carried out on 14 late oral radiation toxicity patients and 5 age-matched volunteers (with no relevant comorbidities in the oral cavity), so far. The demographic and radiotherapy information of the patients is summarized in Table 1.

Each imaging session took about 30–45 min, including subject preparation, equipment adjustment, and imaging. OCT volumetric datasets of various oral regions (including labial tissue, soft palate, and occasionally tongue) of each patient were acquired and saved for further processing to form three-dimensional (3D) images of tissue volumes.

2.2 System design and image validation

A spectral-domain OCT (SD-OCT) system, operating in the 1310-nm spectral region was built for this study. The system utilizes a superluminescent diode (Superlum Ltd.)

Table 1 Summary of patients' demographic and radiotherapy information.

Patient number	Age	Gender	Tumor location	Tumor stage	Concurrent chemotherapy	Years after radiotherapy	Clinical problem[a]
1	47	M	Tonsil	T4a N1	Yes	4	ORN
2	58	M	Left buccal, alveolus and base of tongue	T4 N2c M0	No	9	Trismus, xerostomia, fibrosis
3	55	F	Tongue	T2 N2b	Yes	2	Neck fibrosis, mucosal changes in cheeks and tongue
4	69	M	Nasopharynx	T1 N0	No	9	Bilateral sensorineural hearing loss
5	73	M	Left base of tongue	T4a N2c M0	Yes	2	Xerostomia, dysphagia, pain in neck and jaw
6	70	F	Sinus	T2 N2b	Yes	7	Neck fibrosis, lymphedema
7	69	M	Maxillary sinus	Not available	Yes	8	ORN
8	61	M	Right tongue base	T4a N2b M0	Yes	2	Neck fibrosis, xerostomia, dysphagia
9	62	F	Right tongue	T1 N0 M0	No	9	ORN
10	53	M	Hard palate, right retromolar trigon	T2 N2b M0	Yes	8	ORN, soft tissue necrosis
11	52	F	Right tongue	T4a N1 M0	Yes	7	ORN, trismus
12	58	M	Right tongue	T2 N2c	Yes	9	Fibrosis of right neck
13	65	M	Left retromolar trigon	T4a N2b M0	No	1	ORN
14	41	M	Nasopharynx	T2 N3	Yes	4	Right hypoglossal weakness

M, male; F, female; ORN; osteoradionecrosis.

[a]At the first visit to the Adult Radiation Late Effects Clinic at the Princess Margaret Hospital, Toronto.

with emission spectrum centered at 1310 nm and spectral bandwidth of ~110 nm as the light source, and a high-performance spectrometer (P&P Optica) connected to a 1024 pixel, 47 kHz CCD camera (SU-LDH Line Scan camera; Sensors Unlimited, Inc.) at the detector end of the system. The SD-OCT system provides axial resolution of 5.1 μm in biological tissues [17, 18]. Images from oral tissue were acquired in the form of 3D datasets corresponding to a volume of 1 mm×1 mm (lateral dimensions)×~1 mm (depth). The acquisition time for each 3D dataset was ~5–7 s.

For this study, an OCT probe was designed and built for *in-vivo* imaging of oral tissues. The probe consisted of three lenses in a lens tube (~1.8 cm in diameter and 17 cm in length), attached to a small box containing the galvanometers for scanning the laser beam to enable 3D imaging [17]. During clinical imaging, the subject sat on a chair and placed the chin and the forehead on the chin-rest and forehead rest, respectively. The imaging probe, covered with a disposable transparent sheet, was then inserted into the oral cavity of the subject. The sheet was changed between subjects to prevent cross-contamination. The imaging probe was mounted on a translation/rotation stage to facilitate adjusting the probe position based on each subject's specific anatomy.

Since acquiring biopsies was not part of the protocol in this clinical study (due to its potential hazards for the subjects), a set of preliminary experiments were completed in order to learn how different oral regions appear in OCT images:

1. OCT images of *ex-vivo* pig oral tissue samples were acquired and compared to histology [17]. Based on the high similarity between pig and human oral tissue [19], results from those preliminary studies helped gaining better understanding of how each of the layers and features in the oral tissue (such as epithelium, lamina propria, submucosa, glands, and vessels) appear in OCT grayscale structural images.
2. OCT *in-vivo* images of healthy volunteers' various oral regions were acquired and the different layers and features were identified drawing on the pig-histology comparative study and previous literature reports [17].

2.3 De-speckling the OCT images

To reduce the speckle noise in the acquired OCT images and highlight the subsurface features and layers, the images were processed using the stochastic speckle compensation algorithm [20]. This approach employs a non-stationary spline-based speckle noise modeling strategy to characterize the speckle noise. Based on this learned speckle noise model, a stochastic speckle noise compensation approach via a spatially-adaptive Monte Carlo sampling strategy was then used to estimate the noise-free OCT images. An OCT image of the labial tissue (with its inherent speckle) and the de-speckled version of the same image are shown in Figure 1A and B. Both the epithelium and lamina propria appear more homogeneous in the de-speckled image (Figure 1B). Moreover, the delineation between these two layers (marked with pair of thin arrows) is clearer and the features at the deeper parts of the image (marked with pair of thick arrowheads) are better visualized in Figure 1B. In the de-speckled image, the blood vessels are more easily identifiable since in conventional OCT images, they can be obscured in the background speckles and thus become hard to identify.

2.4 Analysis method

The de-speckled OCT images acquired from various oral regions of healthy volunteers were used to build up an OCT atlas of healthy oral structure. Afterwards, the OCT images of different oral regions in the patients were compared to the atlas. Detectable changes in the morphological features and layer definitions were noted. The alterations in the OCT structural images of each oral region were then correlated with the dose received by that region as predicted by the patient-specific treatment plan. To label different features of the oral tissue, a single OCT B-scan, which is two-dimensional (2D), was not enough. Therefore, numerous consecutive B-scans from the 3D tissue volume were examined and evaluated in order to help identify various subsurface layers and features. Therefore, even though representative 2D OCT cross-sectional images are shown in this manuscript, the ensemble of the consecutive 2D images is the more informative and appropriate tool to help the clinician and researcher to visualize late radiation toxicity effects [17].

3 Results

Representative OCT images of healthy human oral tissue (labial, soft palate, and dorsal tongue) and standard histology of the same oral regions (courtesy of Dr. William J. Krause, Department of Pathology and Anatomical Sciences, University of Missouri) are shown in Figure 2A–I. The section of the labial tissue that was imaged in the human subjects typically consists of an epithelial layer which is not very thick [21]. In the OCT images (Figure 2B and C), this is observed as the low-scattering, dark layer

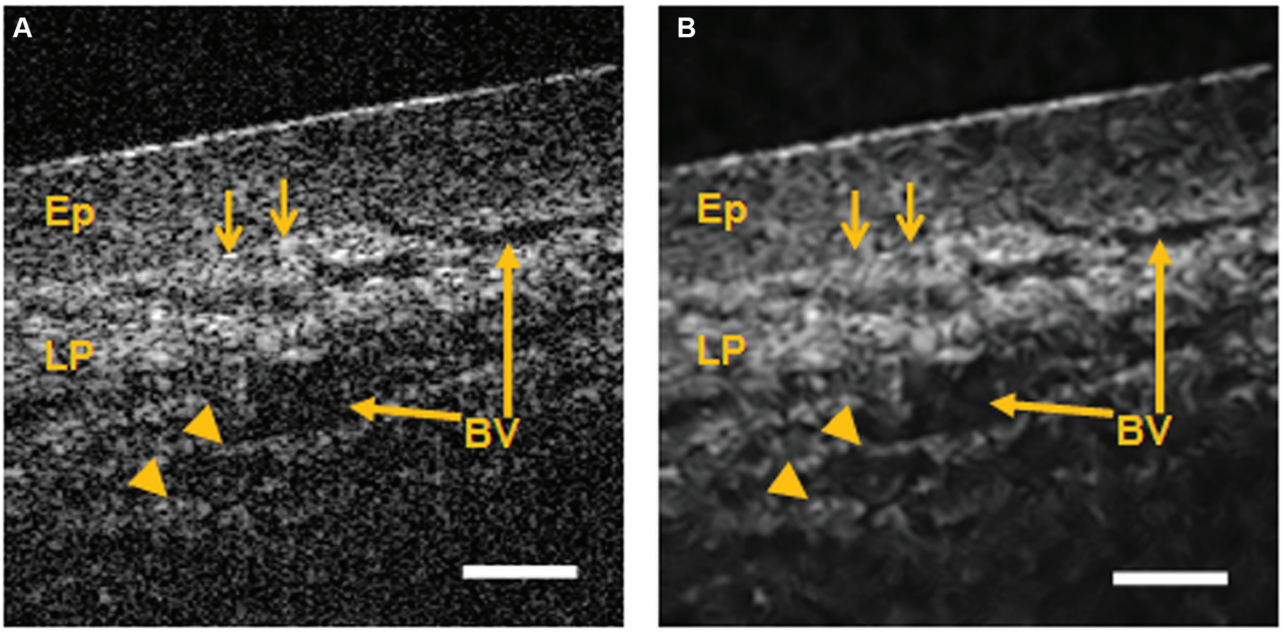

Figure 1 OCT image of the labial tissue of a low-dose region in a patient, (A) before and (B) after applying the de-speckling algorithm. In (B), the epithelium (*Ep*) and lamina propria (*LP*) appear more homogeneous and smooth compared to (A) due to absence of speckles in (B). The blood vessels (*BV*) are more emphasized and better delineated in (B). Deeper layers of the tissue (shown with pair of arrow heads) are visualized after de-speckling and a clearer distinction between the epithelium and lamina propria (shown with pair of thin arrows) are possible. Scale bars: 200 μm.

on top. The lamina propria layer, right below the epithelium, is generally rich in collagen fibers and vasculature [21]. The dense connective tissue appears as a highly-scattering bright layer. The lateral cross-section of the vasculature appears as highly absorbing dark lines throughout this layer. The submucosa should theoretically appear as a highly-scattering layer due to presence of collagenous tissue [21]; however, if visible at all, it does not appear as bright as the lamina propria as it is less dense and also due to light intensity attenuation when it reaches deeper into the tissue. In the soft palate (Figure 2E and F), the epithelium and lamina propria appear similar to labial tissue, but the epithelium is slightly thinner. The penetration depth of OCT does not allow visualization of the submucosa in soft palate; however, an elastin layer is visible underneath the lamina propria right above the submucosa. The elastin layer is specific to the soft palate tissue [21] and can be seen as a dark layer filled with short bright streaks demonstrating the highly scattering elastin fibers. Figure 2H and I show OCT images of the dorsal tongue. This type of oral tissue is histologically characterized by a thick keratinized epithelium formed into papillae structures, with a relatively thick lamina propria underneath [21]; however, because of the strong light scattering from the tongue surface (due to the shape of the papillae), only the epithelium layer can be visualized in the OCT images, with insufficient light reaching the lamina propria for its proper visualization.

Figure 3 shows six de-speckled OCT images from three different regions (labial, soft palate, and dorsal tongue) in several patients. Each region received a different radiation dose. Figure 3A demonstrates the labial tissue in a patient who was diagnosed with fibrosis and trismus (inability to open the mouth). This patient was treated with a total dose of slightly more than 70 Gy in the pre-IMRT era. Therefore, the entire oral cavity received approximately this dose. Comparison of this image to the two representative images from the atlas of healthy labial tissue (Figure 2B and C) shows complete loss of layer definition. Figure 3B shows the labial tissue in another patient. The total dose to this region was between 30 and 50 Gy. As illustrated, the epithelium and lamina propria are still distinguishable and the layer definition and light penetration are similar to those of healthy labial tissue (Figure 2B and C). Figure 3C shows a soft palate that received slightly more than 70 Gy according to the radiation dose plan. Even though the epithelium and lamina propria are distinguishable, the latter is quite thin compared to normal cases (Figure 2E and F). Moreover, the invisibility of the elastin layer also suggests reduced light penetration, possibly due to fibrosis leading to more light scattering and lower penetration depth. Figure 3D demonstrates the soft palate of a patient that received slightly more than 60 Gy during the radiotherapy. A partial layer disruption and reduced light penetration depth can be detected in this case. Figure 3E shows the dorsal tongue of

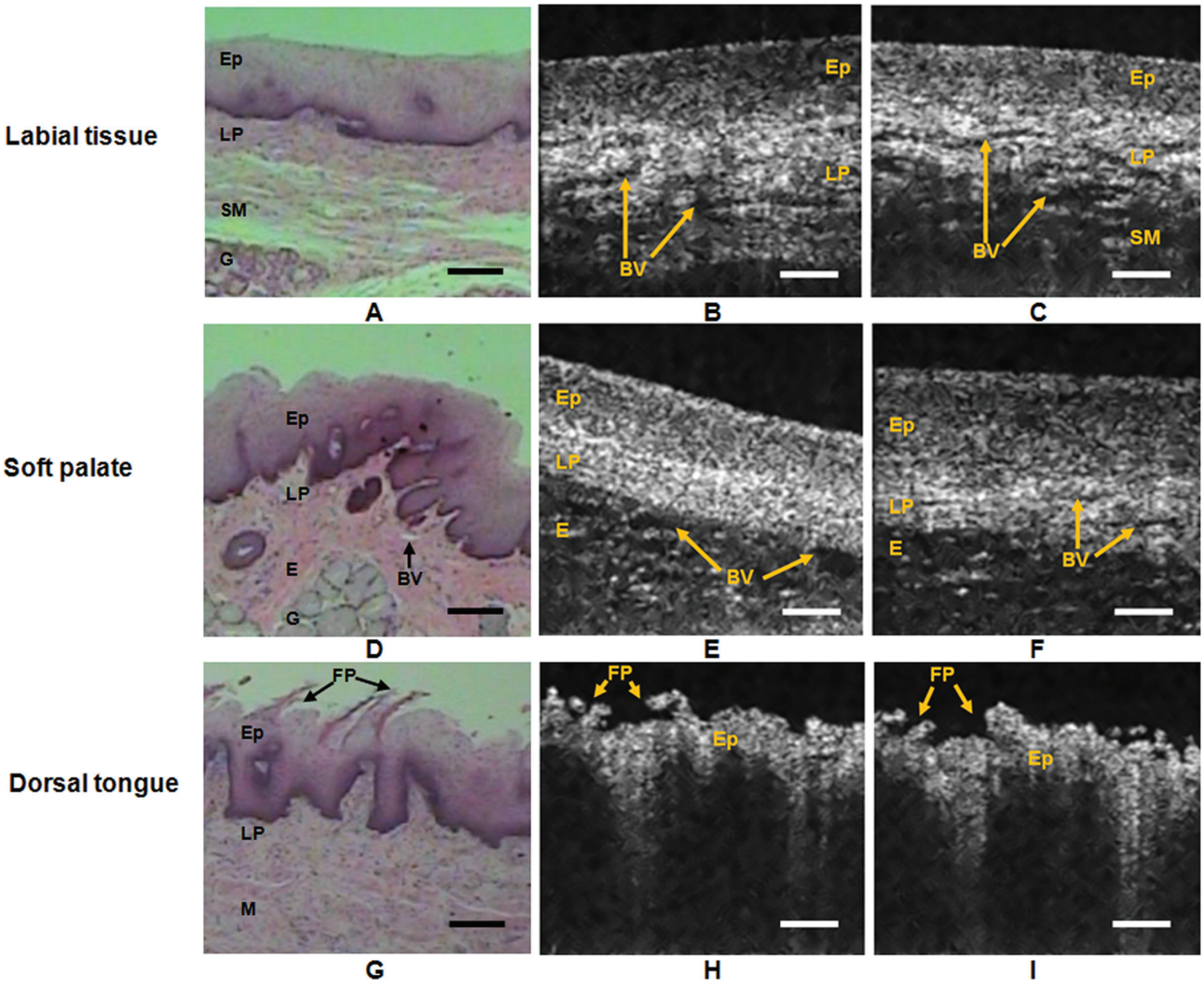

Figure 2 Standard hematoxylin and eosin (H&E)-stained histology slides (left column) and de-speckled OCT images (middle and right columns) of healthy oral tissue: (A–C) labial tissue, (D–F) soft palate, and (G–I) dorsal surface of the tongue. Each of the two OCT images from the same oral site belongs to a different healthy volunteer. In (B, C, E, and F), the epithelium (*Ep*) is the low-scattering dark layer on top with the highly scattering bright lamina propria (*LP*) underneath. The dark narrow lines in this layer are the lateral cross-section of blood vessels (*BV*). The submucosa (*SM*) is visible only in (C). The glands (*G*) that are visible in the H&E histology slide, while sometimes visible in OCT images, cannot be detected in these sample OCT images. In (E and F), the elastin layer (*E*) is noticeable as a dark layer with short bright streaks, right below the lamina propria. In (H and I), the keratinized epithelium and the filiform papillae (*FP*) are visible, while the deeper layers, such as lamina propria and skeletal muscle (*M*) that are visible in the H&E histology, are not visible in OCT images due to limited light penetration into the tongue because of high surface scattering. Scale bars: 200 μm. (Histology slides: courtesy of Dr. William J. Krause, Department of Pathology and Anatomical Sciences, University of Missouri.)

a patient with a tumor in the base of the tongue, treated to about 60–70 Gy. Comparison of this image to representative OCT images of healthy tongue dorsal (Figure 2H and I) suggests a slight loss of the papillae on the tongue surface and a decrease in the light penetration depth into the tissue (which can be related to an increase in collagenous tissue due to fibrosis). Figure 3F shows the dorsal tongue of another patient treated to dose of ~53 Gy. In this case, the deeper light penetration and the presence of papillae (in contrast to Figure 3E) are similar to the features in a healthy dorsal tongue. The one noticeable deviation from healthy dorsal tongue is the tissue desquamation appearing on the tongue surface of this patient.

Figure 4 demonstrates images from the contralateral (non-tumor side, lower dose levels) and ipsilateral (tumor side, full dose levels) soft palate of a late oral radiation toxicity patient. The dose received by the contralateral and ipsilateral sides were <25 Gy and 60–70 Gy,

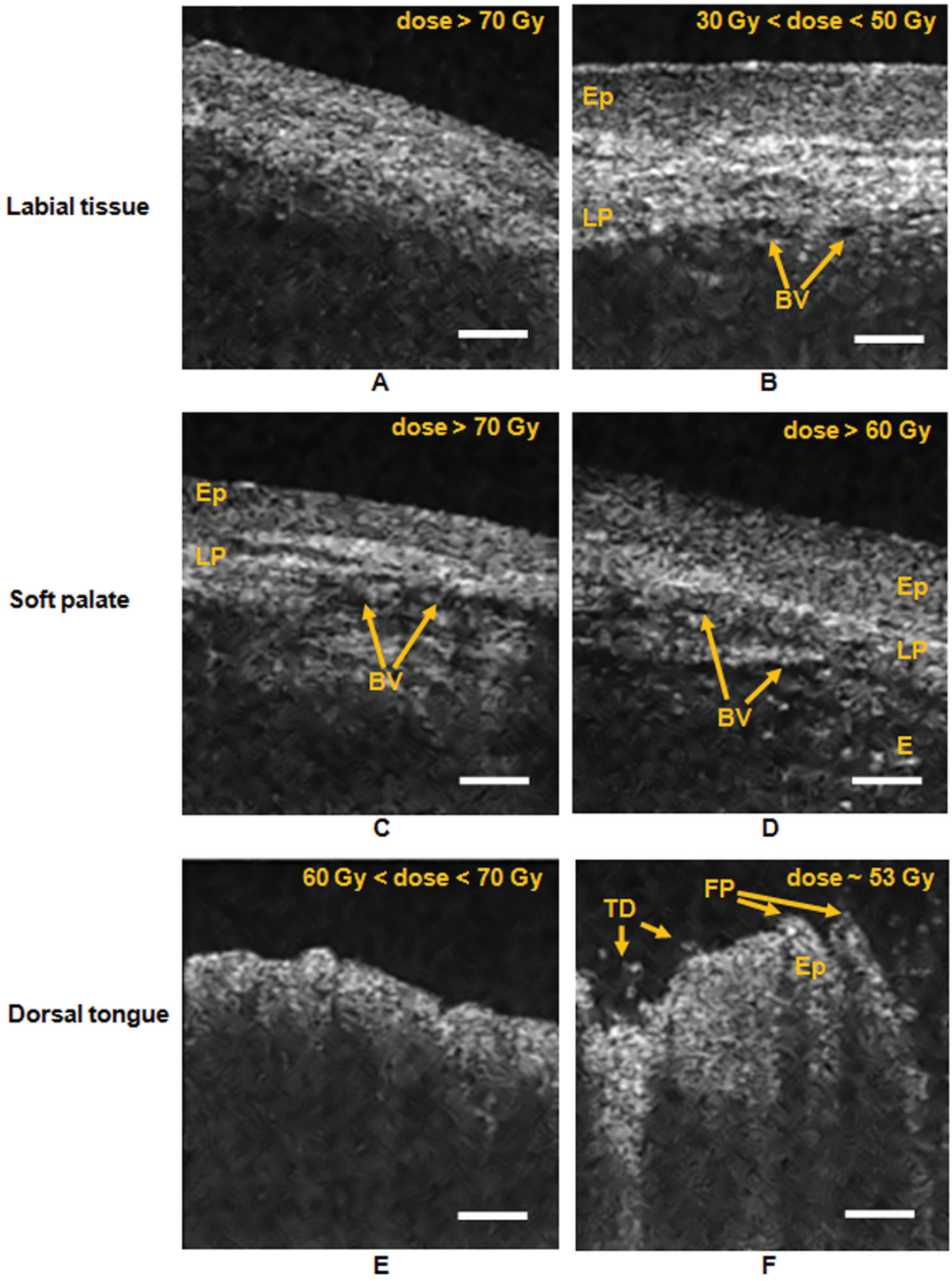

Figure 3 De-speckled OCT images of (A and B) labial tissue; (C and D) soft palate; and (E and F) dorsal tongue of various late oral radiation toxicity patients. (A) Labial tissue of a patient treated in the pre-IMRT era. No distinction between the epithelium (*Ep*) and the lamina propria (*LP*) can be made. Light penetration is reduced due to increased fibrous tissue (fibrosis). (B) Labial tissue that received between 30 and 50 Gy. The well-differentiated epithelium and lamina propria, and the vascularization level of the latter suggest a healthy/well-healed labial tissue. (C) Soft palate treated to a dose slightly higher than 70 Gy. Despite of distinctive epithelium and lamina propria, lack of a visible elastin layer (*E*) as well as thinned epithelium suggests a non-complete or partially-healed soft palate. (D) Soft palate of a patient which received slightly higher than 60 Gy. Medium disruption of layers is detectable. (E) Dorsal tongue of a patient that received about 60–70 Gy, resulting in loss of papillae and a decrease in light penetration depth due to a possible increase in the fibrous content of the tissue (fibrosis). (F) Dorsal tongue of a patient treated to ~53 Gy, with the filiform papillae (*FP*) present and a penetration depth similar to healthy cases. A slight tissue desquamation (*TD*) is present. Scale bars: 200 μm.

respectively. In Figure 4A, the soft palate looks quite healthy, showing distinct epithelium, lamina propria, and elastin layer, with a well-vascularized lamina propria. However, in Figure 4B, the epithelium and lamina propria have become indistinguishable, with no visualization of the elastin layer. The clinician reported "sloughing" of the mucosa of the palate, which is also visible in the OCT images of the ipsi- and contralateral sides and more pronounced on the former.

A summary of the observed features in structural OCT images of different regions in each patient and the total dose to each of those regions is provided in Table 2. For five out of 14 cases, the comparison between these two parameters was not possible due to either absence of patient's dose plan in the hospital's online database, or because of the intolerability of the imaging procedure for specific patients. In the nine remaining cases for which the OCT images were correlated with the radiation dose plan, a total of 32 regions were reviewed. Among these, all 15 regions that received more than 50 Gy (between 50 to slightly more than 70 Gy) showed abnormality in the OCT images (such as disrupted layer definition, reduced light penetration, and tissue desquamation). Among the remaining 17 regions, which received lower than 50 Gy (mean dose ~35 Gy), only one showed abnormality.

4 Discussion

The ability of OCT to image subsurface layers of healthy human oral tissue [22] as well as early side effects of chemotherapy (somewhat similar to those of radiotherapy) in animal models has previously been demonstrated [12, 13, 15]. The suitability of this imaging technique for correlating OCT images of early toxicity (after different radiation doses) to the toxicity grade (using standard clinical scoring systems, such as RTOG) has been shown in a single clinical feasibility study [14]. Due to the much higher negative impact of late radiation toxicity on quality of life, the current study focused on applying OCT to monitor late oral radiation side effects and correlating the acquired images of various oral sites to the total dose delivered to each.

Results showed that the OCT images of the examined regions (including labial, soft palate, and dorsal tongue tissue) which received more than 50 Gy showed a major

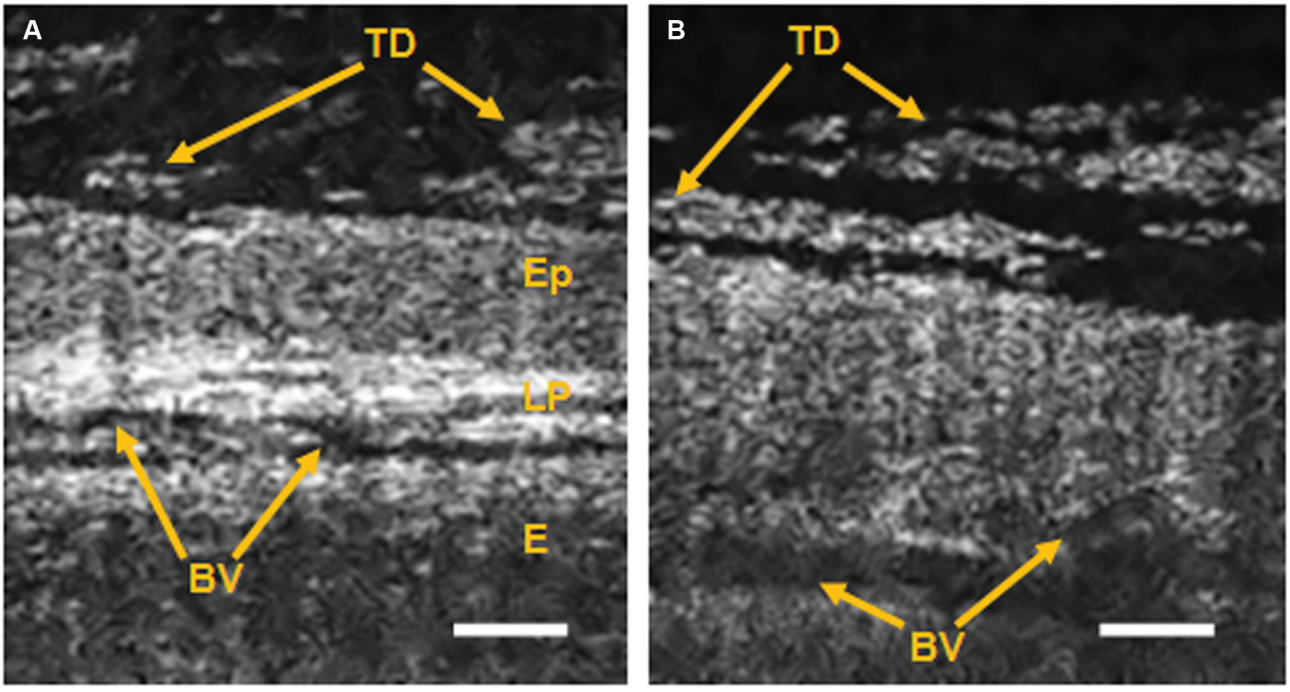

Figure 4 De-speckled OCT images of (A) contralateral (dose <25 Gy) and (B) ipsilateral (dose >70 Gy) soft palate of a late oral radiation toxicity patient. In (A), the soft palate appears as normal with a clear delineation of the epithelium (*Ep*), lamina propria (*LP*) and elastin (*E*) layers. The lamina propria has abundant blood vessels (*BV*). Tissue desquamation (*TD*) is clear on the surface (more severe on the ipsilateral, higher-dose side). In (B), no distinction between the epithelium and lamina propria is possible and the elastin layer cannot be visualized. Scale bars: 200 µm.

Table 2 Summary of the total delivered dose to each oral region and the observed features in the corresponding OCT images.

Patient number	Primary tumor location	Dose (Gy) to					
		Labial R	Labial L	Soft palate R	Soft palate L	Dorsal tongue R	Dorsal tongue L
1	Tonsil	$<30^{N}$	$<30^{N}$	$>63^{P}$	$\sim 50^{P}$	–	–
2	Left buccal, alveolus and base of tongue	$>70^{O}$	$>70^{O}$	IA	IA	$>70^{R,L}$	$>70^{R,L}$
3	Tongue	$<30^{N}$	–	IA	IA	$>66^{R,L}$	–
4	Nasopharynx	Dose plan not available					
5	Left base of tongue	$<35^{N}$	$<35^{N}$	$>60^{P}$	$>70^{O}$	–	–
6	Sinus	$<35^{N}$	$<35^{N}$	IA	IA	$>56^{N,D}$	$>45^{N}$
7	Maxillary sinus	Dose plan not available					
8	Right tongue base	$<50^{N}$	$<50^{N}$	$>66^{P}$	$>56^{P}$	–	–
9	Right tongue	$<50^{N}$	$<50^{N}$	$>60^{P,R}$	$<50^{N}$	–	–
10	Hard palate, right retromolar trigon	$<40^{N}$	$<40^{N}$	$>70^{N,E}$	$<40^{N}$	–	–
11	Right tongue	No useful images acquired due to patient's request for early termination of imaging					
12	Right tongue	Dose plan not available					
13	Left retromolar trigon	–	–	$<25^{N,D}$	$>70^{O,D}$	–	–
14	Nasopharynx	–	–	$\sim 50^{P}$	$\sim 50^{P}$	–	–

R, Right side; L, Left side; IA, Inaccessible side; –, No OCT images acquired from the region due to limited imaging time.
Features in OCT images: ^{N}Normal layer distinction; ^{P}Partial (low/medium) layer distinction; ^{O}No layer distinction; ^{E}Epithelial atrophy; ^{R}Reduced light penetration; ^{L}Lack of/less papillae; ^{D}Tissue desquamation.

difference compared to the images of healthy oral tissue, such as total layer disruption (Figure 3A and E and Figure 4B), reduced layer distinction (Figure 3D), change in subsurface layer thickness (Figure 3C), change in light penetration depth (Figure 3A and E), loss of papillae structure (Figure 3E), and tissue desquamation (Figure 3F). The severity of these complications, however, was not the same in different patients that received the same dose, as it can vary based on factors such as the phenotype and location of primary tumor, each patient's biological response to radiation, and the medication each patient received for the complications. Despite these confounding factors, the result of this study showed that the threshold dose of ~50 Gy, previously noted in the literature [23] as the threshold for onset of most late radiation side effects, resulted in late complication in the subjects under study. Further, to show that the observed abnormalities in the patients (Figure 3) compared to healthy volunteers (Figure 2) were not merely due to anatomical differences between individuals, an example (Figure 4) was used to show that the same abnormalities occurred in the OCT images of the ipsilateral soft palate (dose >70 Gy) of one of the patients, while the images of the contralateral side (dose <25 Gy) of the same patient demonstrated essentially normal features.

Apart from tissue structural damage, vascular damage has been shown to play an important role in radiation toxicity, especially in late effects [23, 24]. Changes in vessel morphology and blood flow characteristics in radiation toxicity (early and late) have been studied by a few groups, including our own, with microvascular OCT [15, 18] or other imaging techniques [25–28]. Using only structural OCT images (such as in the current study) has the disadvantage that apart from the presence or absence of blood vessels in general, it does not provide any information on blood flow or vessel morphology-related metrics. However, this study was decided to be focused on structural OCT images because of the ready availability of OCT systems with structural imaging capability, since the implementation of vascular detection techniques (such as Doppler and speckle variance-based methods) can be complicated and may not be available in simple clinical systems. Therefore, using OCT systems with structural imaging capability and applying image processing methods (such as the de-speckling technique used in this study) can provide a low cost, real-time and easy-to-use system for detection of radiation-induced oral subsurface abnormalities in the clinical or research scenario.

The current study can be extended to a prospective cohort study that monitors the dose-related biological alterations as the dose accumulates during radiotherapy (early radiation toxicity) and longitudinally following the therapy (e.g., every several months to visualize late radiation toxicity). Such a prospective study would potentially allow a more thorough monitoring of radiation-induced subsurface alterations as a function of total dose over time, leading to a better understanding of the progression and mechanism of late radiation complications *in-vivo*.

5 Conclusion

Structural alterations in different oral regions of late oral radiation toxicity patients were shown to appear in the de-speckled OCT images of the regions which received doses >50 Gy. There are major factors such as difference in initial pathologies among the patients, various responses to radiation, and the treatment each had received for their radiation toxicity that impact the severity of anatomical changes in the OCT images. However, the impact of the total dose cannot be neglected. The fact that specific anatomical changes were seen majorly after accumulation of a certain dose can guide the design of future prospective cohort studies on dose dependent onset of late oral radiation toxicity. Such a prospective study on monitoring head-and-neck cancer patients every several months following their radiotherapy can "shed light" on the mechanism of late oral radiation toxicity and how it is related to the total dose to different oral sites.

Acknowledgments: The authors would like to thank the Natural Sciences and Engineering Research Council of Canada (NSERC)/Collaborative Health Research Program (CHRP), the University Health Network (UHN) Toronto, Canada, and the Ministry of Education and Science of the Russian Federation (grant 14.B25.31.0015) for funding this research. We also extend our acknowledgment to Dr. William J. Krause at the Department of Pathology and Anatomical Sciences, University of Missouri for giving us the permission to use his archive of oral histology slides.

Conflict of interest statement: There are no financial and commercial conflicts of interests to report.

References

[1] Chao KS, Majhail N, Huang CJ, Simpson JR, Perez CA, Haughey B, Spector G. Intensity-modulated radiation therapy reduces late salivary toxicity without compromising tumor control in patients with oropharyngeal carcinoma: a comparison with conventional techniques. Radiother Oncol 2001;61(3):275–80.

[2] Sciubba JJ, Goldenberg D. Oral complications of radiotherapy. Lancet Oncol 2006;7(2):175–83.

[3] Specht L. Oral complications in the head and neck radiation patient. Introduction and scope of the problem. Support Care Cancer 2002;10(1):36–9.

[4] Stone HB, Coleman CN, Anscher MS, McBride WH. Effects of radiation on normal tissue: consequences and mechanisms. Lancet Oncol 2003;4(9):529–36.

[5] Denis F, Garaud P, Bardet E, Alfonsi M, Sire C, Germain T, Bergerot P, Rhein B, Tortochaux J, Oudinot P, Calais G. Late toxicity results of the GORTEC 94-01 randomized trial comparing radiotherapy with concomitant radiochemotherapy for advanced-stage oropharynx carcinoma: comparison of LENT/SOMA, RTOG/EORTC, and NCI-CTC scoring systems. Int J Radiat Oncol Biol Phys 2003;55(1):93–8.

[6] Small Jr. W, Woloschak GE, editors. Radiation toxicity: a practical guide. New York: Springer Science+Business Media. LLC; 2006.

[7] Drexler W, Fujimoto JG, editors. Optical coherence tomography technology and applications. Berlin: Springer; 2008.

[8] Yang V, Gordon M, Qi B, Pekar J, Lo S, Seng-Yue E, Mok A, Wilson B, Vitkin I. High speed, wide velocity dynamic range Doppler optical coherence tomography (Part I): system design, signal processing, and performance. Opt Express 2003;11(7):794–809.

[9] Mariampillai A, Leung MK, Jarvi M, Standish BA, Lee K, Wilson BC, Vitkin A, Yang VX. Optimized speckle variance OCT imaging of microvasculature. Opt Lett 2010;35(8):1257–9.

[10] Lee CK, Tsai MT, Lee HC, Chen HM, Chiang CP, Wang YM, Yang CC. Diagnosis of oral submucous fibrosis with optical coherence tomography. J Biomed Opt 2009;14(5):054008.

[11] Tsai MT, Lee CK, Lee HC, Chen HM, Chiang CP, Wang YM, Yang CC. Differentiating oral lesions in different carcinogenesis stages with optical coherence tomography. J Biomed Opt 2009;14(4):044028.

[12] Muanza TM, Cotrim AP, McAuliffe M, Sowers AL, Baum BJ, Cook JA, Feldchtein F, Amazeen P, Coleman CN, Mitchell JB. Evaluation of radiation-induced oral mucositis by optical coherence tomography. Clin Cancer Res 2005;11(14):5121–7.

[13] Calantog A, Hallajian L, Nabelsi T, Mansour S, Le A, Epstein J, Wilder-Smith P. A prospective study to assess in vivo optical coherence tomography imaging for early detection of chemotherapy-induced oral mucositis. Lasers Surg Med 2013;45(1):22–7.

[14] Gladkova N, Maslennikova A, Balalaeva I, Feldchtein F, Kiseleva E, Karabut M, Iksanov R. Application of optical coherence tomography in the diagnosis of mucositis in patients with head and neck cancer during a course of radio(chemo)therapy. Med Laser Appl 2008;23(4):186–95.

[15] Wilder-Smith P, Hammer-Wilson MJ, Zhang J, Wang Q, Osann K, Chen Z, Wigdor H, Schwartz J, Epstein J. In vivo imaging of oral mucositis in an animal model using optical coherence tomography and optical Doppler tomography. Clin Cancer Res 2007;13(8):2449–54.

[16] ClinicalTrials.gov identifier: NCT01692600. Optical coherence tomography for monitoring late oral radiation toxicity after radiotherapy of head-and-neck cancer patients. http://www.clinicaltrials.gov/ [Accessed on July 8, 2014].

[17] Davoudi B, Lindenmaier A, Standish BA, Allo G, Bizheva K, Vitkin A. Noninvasive in vivo structural and vascular imaging of human oral tissues with spectral domain optical coherence tomography. Biomed Opt Express 2012;3(5):826–39.

[18] Davoudi B, Morrison M, Bizheva K, Yang VX, Dinniwell R, Levin W, Vitkin IA. Optical coherence tomography platform for microvascular imaging and quantification: initial experience in late oral radiation toxicity patients. J Biomed Opt 2013;18(7):76008.

[19] Wong JW, Gallant-Behm C, Wiebe C, Mak K, Hart DA, Larjava H, Häkkinen L. Wound healing in oral mucosa results in reduced scar formation as compared with skin: evidence from the red Duroc pig model and humans. Wound Repair Regen 2009;17(5):717–29.

[20] Cameron A, Lui D, Boroomand A, Glaister J, Wong A, Bizheva K. Stochastic speckle noise compensation in optical coherence tomography using non-stationary spline-based speckle noise modelling. Biomed Opt Express 2013;4(9):1769–85.
[21] Squier C, Brogden KA. Human oral mucosa: development, structure, and function. Chichester: Wiley-Blackwell; 2011.
[22] Ridgway JM, Armstrong WB, Guo S, Mahmood U, Su J, Jackson RP, Shibuya T, Crumley RL, Gu M, Chen Z, Wong BJ. In vivo optical coherence tomography of the human oral cavity and oropharynx. Arch Otolaryngol Head Neck Surg 2006;132(10):1074–81.
[23] Fajardo LF, Berthrong M, Anderson RE. Radiation pathology. New York: Oxford University Press, Inc.; 2001.
[24] Baker DG, Krochak RJ. The response of the microvascular system to radiation: a review. Cancer Invest 1989;7(3):287–94.
[25] Dimitrievich GS, Fischer-Dzoga K, Griem ML. Radiosensitivity of vascular tissue. I. Differential radiosensitivity of capillaries: a quantitative in vivo study. Radiat Res 1984;99(3):511–35.
[26] Hamilton S, Yoo J, Hammond A, Read N, Venkatesan V, Franklin J, Fung K, Gray D, Parry N, Van Diepen K, Baswick BL, Badhwar A. Microvascular changes in radiation-induced oral mucositis. J Otolaryngol Head Neck Surg 2008;37(5):730–7.
[27] Juan CJ, Chen CY, Jen YM, Liu HS, Liu YJ, Hsueh CJ, Wang CY, Chou YC, Chai YT, Huang GS, Chung HW. Perfusion characteristics of late radiation injury of parotid glands: quantitative evaluation with dynamic contrast-enhanced MRI. Eur Radiol 2009;19(1):94–102.
[28] Reinhold HS. The influence of radiation on blood vessels and circulation. Chapter IV. Structural changes in blood vessels. Curr Top Radiat Res Q 1974;10(1):58–74.